Twin and tweed microstructures in $YBa_2Cu_3O_{7-\delta}$ doped by trivalent cations

S. Semenovskaya
Department of Materials Science, Rutgers University, P.O. Box 909, Piscataway, New Jersey 08855-0909

Yimei Zhu and M. Suenaga
Division of Materials Science, Brookhaven National Laboratory, Upton, New York 11973

A. G. Khachaturyan
Department of Materials Science, Rutgers University, P.O. Box 909, Piscataway, New Jersey 08855-0909
(Received 30 October 1992)

Computer-simulation techniques and TEM analysis were employed to study the dependence of the twin and tweed microstructures in $YBa_2Cu_{3-x}M_xO_{7-\delta}$ on doping by trivalent atoms (like Fe, Co, or Al). Since the trivalent atoms substituting the bivalent Cu(I) atoms have a greater number of the nearest-neighbor oxygen atoms, it was suggested that doping can be described by the M-O nearest-neighbor attractive interaction. This interaction generates a local oxygen disorder which plays an important role in the formation of the tweed structure. The M-O interaction and the long-range O-O interaction (screened Coulomb and strain induced) were taken into account to simulate the oxygen ordering kinetics. The simulation is based on equations describing the microscopic diffusion of oxygen atoms. The obtained simulated microstructures are in qualitative and even quantitative agreement with electron microscopic observations for $YBa_2Cu_{3-x}Fe_xO_{7-\delta}$ and with previous electron microscopic data. Both the computer simulations and the TEM results have shown that the usual twin structure, formed through coarsening and refining of the transient tweed structure, is produced at small doping ($x \leq \sim 0.08$). At larger x ($\sim 0.08 < x < \sim 0.2$–0.3), the dopant atoms prevent coarsening and a metastable (or stable) mesoscopic tweed pattern appears. Although the crystal lattice is locally distorted by ultrafine orthorhombic domains forming the tweed pattern, the average crystal lattice determining the diffraction spot pattern is tetragonal. At higher x, the ultrafine orthorhombic domains producing the tweed structure disappear and a disordered tetragonal phase is formed. It is found that doping does not affect the microstructure if the long-range model for the M-O interactions is assumed.

I. INTRODUCTION

Any phase transformation reducing the crystal-lattice point symmetry results in a misfit between the crystal lattices of parent and product phases and between the different orientation variants of an ordered phase (structural domains). Accommodation of the elastic strain induced by the misfit causes the structural instability of a single domain state of the product phase with respect to the formation of a coherent mixture of its twin-related orientation variants. These orientation variants should form a polytwin structure.[1–5] Actually, this structural instability is a result of the strain-induced dipole-dipolelike interaction between the finite elements of the product phase.[3] Typical examples of such transformations are the fcc→bcc martensitic transformation where the Bain transformation strain has the tetragonal symmetry, cubic→tetragonal martensitic transformations as well as any congruent ordering reaction resulting in the reduction of the point group symmetry (for example, fcc CuAu→fct CuAu I). A good and important generic example of the ordering system where the transformation reduces the point symmetry of a parent phase is the high-temperature superconducting $YBa_2Cu_3O_{7-\delta}$ undergoing the tetragonal→orthorhombic transition. The structure transformations in this system will be considered below.

The stable polytwin morphology does not necessary form at once. As has been shown by the authors,[4,5] the oxygen ordering in pure $YBa_2Cu_3O_{7-\delta}$ compound producing the transformation from the tetragonal T phase to the orthorhombic O(I) phase eventually generates the (110) polytwin structure through the strain-induced coarsening and refining the intermediate transient tweed structure. This transient structure is called the primary tweed since it forms due to the primary $T \rightarrow$O(I) ordering reaction. The primary tweed structure pattern consists of microdomains of two orientation variants of the orthorhombic O(I) phase with a strong alignment along the ⟨110⟩ directions.

It is, however, interesting that the transient tweed structure becomes metastable if the secondary ordering reaction O(I)→O(II) occurs.[5] This ordering transforms the domains of the O(I) phase into domains of the O(II) phase. The secondary tweed consisting of two orientation variants of microdomains of the O(II) orthorhombic phase is metastable since after a certain "annealing" time it does not evolve any more. Because orientation variants of the secondary tweed are formed from those of the primary tweed, they are also aligned along the ⟨110⟩ direc-

tions. Therefore, the mesoscopic patterns of the primary and the secondary tweed are geometrically identical although they are formed by microdomains of different orthorhombic ordered phases.

The tweed pattern was first discovered in Cu-Be alloys by Tanner[6] and later was reported in many systems undergoing the phase transformation with the reduction of the crystal lattice symmetry (see, for example, Refs. 7 and 8). It has been demonstrated that the tweed formation mechanism is associated with the self-accommodation of the elastic strain induced by the phase transformation.[3,9,10]

As been found recently by the authors[11,12] and in Refs. 13 and 14, the stable tweed pattern is also observed in superconducting $YBa_2Cu_{3-x}M_xO_{7-\delta}$ doped by trivalent atoms M which substitute Cu atoms (where M = Fe, Co, and Al). The tweed pattern in M-doped material seems to have nothing to do with the diffusion of M atoms. The latter follows from the observation that oxygen reduction and reoxidation at 400 °C (where the mobility of M atoms is very low) results in disappearing and reappearing the tweed pattern.[12] It was shown that the increase of the dopant content x changes the ultimate microstructure from a thick twin structure to a thin twin structure and finally to the tweed structure. At higher x, the tweed structure disappears and a disordered tetragonal structure with a short-range order is formed. The minimum stoichiometry x_0, above which the ultimate twinned microstructure becomes the tweed one, was found to be near 0.08 [$x_0 < 0.09$ (Ref. 11) for Fe-doped and $x_0 \sim 0.07-0.06$ (Refs. 13 and 14) for Co-doped $YBa_2Cu_{3-x}M_xO_{7-\delta}$]. The upper border x_1, above which the tweed microstructure and tweed-induced diffraction pattern disappear, is around ~ 0.3 for Fe-doped oxides.[11,12] Hereafter, the stoichiometry x is defined by the formula $(Cu_{3-x}M_x)$ rather than by the formula $(Cu_{1-x}M_x)_3$ used in Refs. 11–14.

As far as we know, the question why the trivalent doping causes such a dramatic change in the microstructure is still not completely resolved. However, experimental studies, based on the different methods, x-ray-absorption-fine-stucture, Mössbauer, thermogravimetry, neutron diffraction, and others (see, for example, Refs. 15–25), resulted in certain generally accepted conclusions.

(a) Trivalent M atoms, like Co, Fe, and Al, substitute mainly Cu(1) atoms in Cu-O planes [in (001) basal planes].

(b) At the substitution of a dopant M-atom for a Cu(I) atom, the in-plane nearest-neighbor oxygen coordination number for M atom increases from 2 to ~ 3. Extra oxygen atoms should occupy the "wrong" a sites nearest to the M atom because there are only two "right" sites nearest to the M atom which are along the b axis in the Cu-O plane. Appearance of O atoms in the "wrong" sites along the a axis results in disordering.

(c) Doping changes the interaction parameters and lengths of different bonds producing the asymmetric lattice distortions around M atoms, it also gives considerable changes in the unit cell volume and the lattice parameters. There are also the theoretical works (see, for example, Refs. 26–28) where the doping effect was analyzed in terms of a simple model describing the change of interatomic interaction.

The main purpose of this work is an attempt to explain why and how the doping of $YBa_2Cu_3O_{7-\delta}$ by trivalent cations changes the mesoscopic structure pattern. It is shown that even a simple phenomenological model, which takes into account the most important features distinguishing the interaction in ceramic oxides from that in the metal compounds, is able to describe correctly the main qualitative and even the quantitative characteristics of the structure transformations in doped $YBa_2Cu_3O_{7-\delta}$. These features are the long-range electrostatic and strain-induced O-O interactions, and the presence of a short-range M-O interaction related to covalent bonding. As is shown below, the local perturbation caused by the M-O interaction, actually, describes the doping effect.

To test the ability of different theoretical models to describe the observed phenomenon, we use both the computer simulation and new TEM results for Fe-doped $YBa_2Cu_3O_{7-\delta}$. The computer simulation and electron microscopy techniques are the same as those employed in previous works[4,5] and Refs. 11, 12, and 29–31, respectively.

II. COMPUTER SIMULATIONS OF ORDERING

Study of the effect of doping on ordering and microstructure transformations in $YBa_2Cu_{3-x}M_xO_{7-\delta}$ is actually reduced to a study of the oxygen ordering in the Cu-O basal planes in a static external field generated by the dopant-oxygen (M-O) interaction. We assume the M atoms to be immobile. For the O-O interaction, we accepted the same long-range interaction model as that used in our previous works.[4,5] This model describes the O-O interactions as the sum of the anisotropic screened Coulomb interaction proposed by Aligia and coworkers[32,33] and the strain-induced interaction. The model proves to work well for the structure transformation in undoped $YBa_2Cu_3O_{7-\delta}$.[4,5]

We have tested three possible models of the M-O interaction responsible for the doping effect. In testing, we compared at different x the computer-simulated structures with the electron microscopic images. These models assume the following interactions: (i) a long-range attractive M-O electrostatic interaction; (ii) a long-range strain-induced M-O interaction due to the strain effect generated by M atoms (it is related to the macroscopic crystal lattice distortion upon doping); (iii) a nearest-neighbor attractive M-O interaction caused by the covalent bonding responsible for the increase of the number of the nearest-neighbor oxygen atoms around the M atoms.

The employed computer simulation technique is the the same as in Refs. 4 and 5. The M atoms, whose number was chosen in accordance with their stoichiometry x, were randomly distributed over the Cu(I) crystal lattice sites. Diffusion of dopant atoms, as well as the Cu(I) atoms, during the oxygen ordering kinetics was not permitted, and only the oxygen atoms were allowed to move through the diffusional jumps between the closest interstitial sites in the basal (001) Cu-O planes (the nearest-

neighbor interstitial sites belong to two different sublattices whose sites are on the a and b axes, respectively; these sublattices are designated below by indices p, q, or s). The kinetic equation describing the diffusion of O atoms in the potential field generated by dopant atoms is similar to that employed in Refs. 4 and 5. It has the form

$$\frac{d\tilde{n}(p,\mathbf{k};t)}{dt}=\sum_{q=1}^{q=2}\tilde{L}(\mathbf{k})_{pq}\left[\left[\sum_{s=1}^{s=2}[V(\mathbf{k})_{qs}^{f}+B(\mathbf{k})_{qs}]\tilde{n}(s,\mathbf{k};t)\right]+\phi_q(\mathbf{k})c(\mathbf{k})_M\tilde{n}(q,\mathbf{k};t)+k_BT\left[\ln\frac{n(q,\mathbf{r};t)}{1-n(q,\mathbf{r};t)}\right]_{\mathbf{k}}\right], \quad (1)$$

where $\mathbf{r}$ labels the position of Cu(I) (or M) atom nearest to the interstitial site $(p,\mathbf{r})$; functions $\tilde{n}(p,\mathbf{k};t)$, $V(\mathbf{k})_{qs}^{f}$, $B(\mathbf{k})_{qs}$, $\tilde{L}(\mathbf{k})_{pq}$, and

$$\left[\ln\frac{n(q,\mathbf{r};t)}{1-n(q,\mathbf{r};t)}\right]_{\mathbf{k}}$$

are the Fourier transforms of the respective functions: the occupation probability $n(p,\mathbf{r};t)$ to find an oxygen atom in the interstitial site $(p,\mathbf{r})$ at the time t, the pairwise interaction $W(\mathbf{r})_{qs}^{f}$ which includes the anisotropic screened Coulomb but does not include the pairwise strain-induced interaction whose Fourier transform is $B(\mathbf{k})_{qs}$, the matrix $L(\mathbf{r}-\mathbf{r}')_{pq}$ of the kinetic coefficients characterizing the probability of an elementary diffusional jump from the site $(q,\mathbf{r}')$ to the site $(p,\mathbf{r})$, and the entropy-related function

$$\ln\frac{n(q,\mathbf{r};t)}{1-n(q,\mathbf{r};t)}\ .$$

Vector $\mathbf{k}$ is the wave vector within the first Brillouin zone of the disordered T phase, k_B is the Boltzmann constant, and T is the temperature. Equation (1) is, actually, the microscopic extension of the Ginzburg-Landau time-dependent equation.

The only difference of the above equation with the kinetic equation in Refs. 4 and 5 is that Eq. (1) includes the additional term

$$\phi_q(\mathbf{k})c(\mathbf{k})_M\tilde{n}(q,\mathbf{k};t)$$

describing the potential field acting on O atoms from the immobile M atoms. Here, $\phi_q(\mathbf{k})$ is the Fourier transform of the pairwise M-O interaction, $c(\mathbf{k})_M$ is the Fourier transform of the function $c(\mathbf{r})_M$ describing the random distribution of dopant atoms [$c(\mathbf{r})_M=1$ if a site $\mathbf{r}$ is occupied by an M atom and $c(\mathbf{r})_M=0$ if it is occupied by a Cu(I) atom]. The function $c(\mathbf{r})_M$ is chosen so that it provides the dopant content x.

As in Refs. 4 and 5, the computer simulation of the oxygen ordering in (001) Cu-O basal (a-b) plane was realized by numerical solution of kinetic equations (1) (with the same O-O interactions parameters as in Refs. 4 and 5). It allowed us to find the structures formed during the oxygen ordering kinetics. We have studied the $T\rightarrow$O transformation in $YBa_2Cu_2Cu_{3-x}M_xO_7$ with different dopant content x. The $T\rightarrow$O oxygen ordering transformation was simulated by "quenching" the disordered tetragonal T phase to the temperature T_a, which is below the order-disorder transition temperature T_0, and subse-

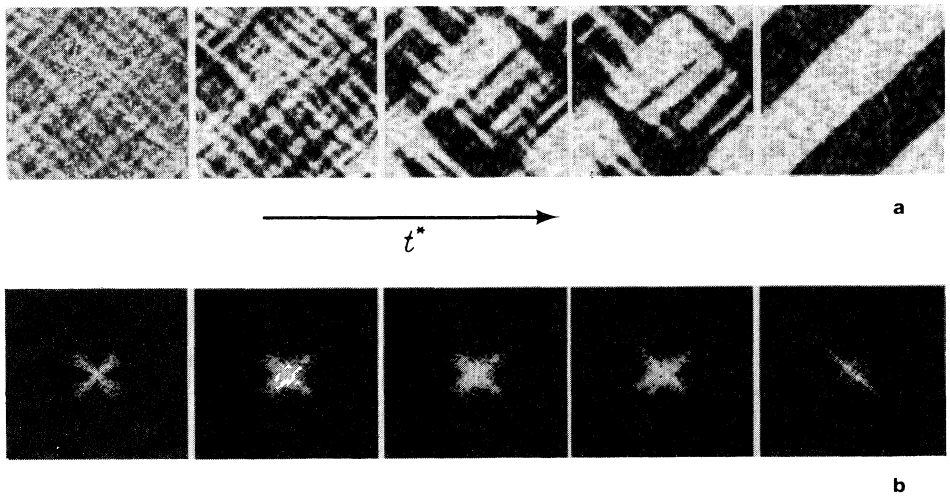

FIG. 1. (a) Simulated temporal isothermal evolution of microstructure in doped $YBa_2Cu_{3-x}M_xO_7$ at $x=0.04$ and the temperature $T_a/T_0=0.79$. The transformation reduced time t^* is equal: 4, 8, 48, 108, 348 (from left to right). The transient tweed structure (at small times $t^*=4$ and 8) obtained along the transformation path from the initial disordered state transforms to the (110) twinned ordered state, therefore, showing the tweed→twin rearrangement. Two types of orientation domains are characterized by the value of the lro parameter $\langle\eta\rangle$ [Eq. (2)]. Black and white colors describe the O(I) ordered domains of two different orientations. Small gray areas are around the positions of dopant atoms. (b) The corresponding strain-induced diffuse scattering around (400) fundamental diffraction spot. The intensity is shown on a logarithmic scale. The system size is 128×128 unit cells.

quent annealing at T_a. For example, structures given in Figs. 1 and 2 correspond to $T_a/T_0=0.79$. They demonstrate the results of the $T\rightarrow$O oxygen ordering for the (iii) model (the nearest-neighbor attractive M-O interaction) after the annealing during the reduced time $t^*=4t/\tau$, where t is the time and τ is the characteristic time of an elementary jump of O atom between the two nearest-neighbor interstitial sites. The initial disordered structure of the T phase was characterized by a random distribution of O atoms over interstitial sites of both sublattices (with sites on a or b axes) with "infinitesimal" fluctuations around the average oxygen concentration $c=0.5$. In this computer simulation, a 128×128 computational cell in a (001) Cu-O basal a-b plane is employed. Since the (001) basal planes are separated by three perovskite unit cells, these two dimensional calculations may be considered as quite a reasonable first approximation (this was confirmed by our previous results[4,5]).

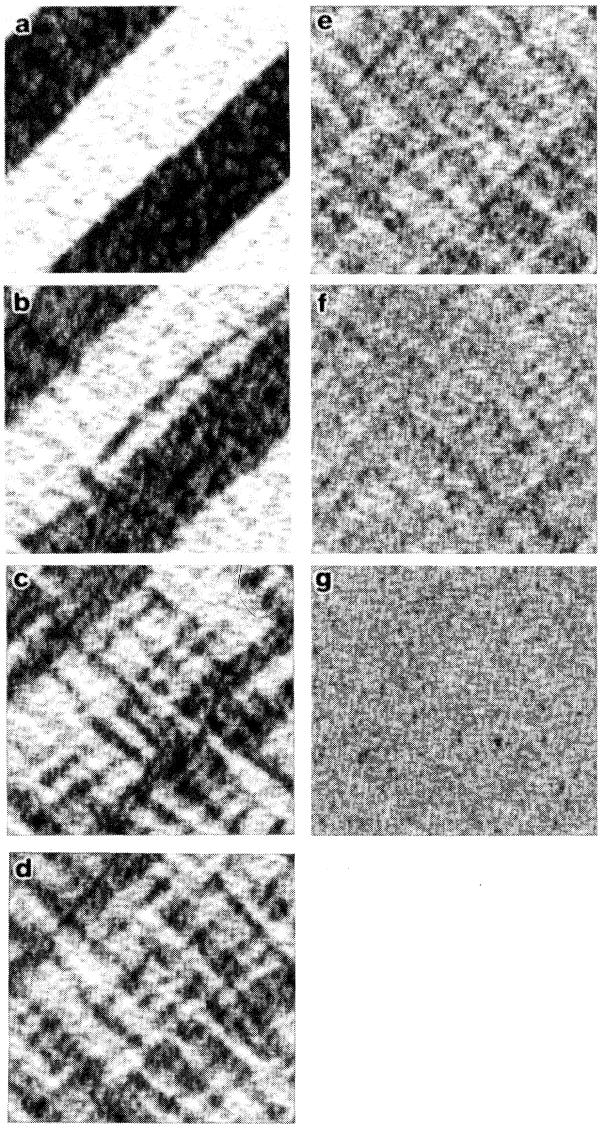

FIG. 2. Simulated microstructures in $YBa_2Cu_{3-x}M_xO_7$ at different dopant content x at the temperature $T_a/T_0=0.79$. The values of x are (a) 0.04, (b) 0.08, (c) 0.10, (d) 0.12, (e) 0.18, (f) 0.24, and (g) 0.40. The transformation reduced time t^* is equal to (a) 348, (b) 408, (c) and (d) 188, (e) 168, and (f) and (g) 48. All conditions are the same as for Fig. 1(a).

Simulations carried out for the possible models (i) and (ii) of the M-O interaction have shown that in the case (i) the long-range screened Coulomb M-O interaction (with M-atom excessive charge being a half of the oxygen charge) does not affect the microstructures formed during the $T\rightarrow$O transformation (only the defects emerge around the M atoms). The structure transformation occurs exactly the same way as in an undoped material, by the formation of a transient primary tweed pattern followed by its rearrangement into the (110) polytwin pattern.

In the case of the model (ii), the M atoms are assumed to be the dilatational "point defects." The dilatational defect results in a symmetrical crystal lattice distortion with the symmetry of the host lattice. The corresponding M-O strain-induced interaction was estimated using the dependence of the crystal lattice parameters of the $YBa_2Cu_2Cu_{3-x}M_xO_7$ on the dopant content x (Ref. 34) and the elastic strain moduli of $YBa_2Cu_3O_7$ (Ref. 35). We found that this interaction changes the microstructure: it decreases the twin spacing at small x and transforms the twin structure into an aligned fine structure with a modulation whose characteristic length strongly decreases with x. These alignments, however, are along the $\langle 100\rangle$ directions rather than the $\langle 110\rangle$ directions observed for the tweed pattern in this compound. Therefore, the M-O interaction described by the model (i) or (ii) is not responsible for the observed microstructures, or its effect is too small to be taken into account.

The nearest-neighbor M-O interaction model (iii) corresponds to a covalent bond formation which certainly takes place when the bivalent Cu(I) atoms are replaced by the trivalent M atoms. This interaction is attractive and of the same order of magnitude as the nearest-neighbor Coulomb interaction,

$$-(z_M^*-z_{\mathrm{Cu}}^*)z_{\mathrm{O}}^*/(a/\sqrt{2}) ,$$

where z_M^*, z_{Cu}^*, and z_{O}^* are the effective charges of M, Cu, and O atoms. Actually, this interaction correctly reproduces the experimentally observed tendency for the increase of the oxygen coordination number of M atoms. Although this model is rather crude (it neglects the multiparticle effect typical for the covalent bonding), it, nevertheless, gave us the results which are in a good agreement with the observed changes of microstructure upon doping.

Some of the computer-simulation results are presented in Figs. 1 and 2 for the particular value of the nearest-neighbor M-O interaction, $W_{M\text{-O}}=-0.17$ eV. To visualize the simulation results, we have to present them in a form which could be compared with the TEM images. Particularly, we used the local long-range order (lro) parameter averaged over the five crystal lattice sites around the site $\mathbf{r}$:

$$\langle\eta\rangle=(\langle n(1,\mathbf{r};t)\rangle-\langle n(2,\mathbf{r};t)\rangle+1)/2 , \quad (2)$$

where $n(p,\mathbf{r};t)$ is the occupation probability to find an O atom in the interstitial site $(p,\mathbf{r})$ at the time t, and the symbol $\langle \cdots \rangle$ designates averaging over the site $\mathbf{r}$ and the four nearest lattice sites, $\mathbf{r}\pm a$ and $\mathbf{r}\pm b$ (where a and b are the unit translations in the directions [100] and [010]). Averaging "smoothes" the lro parameter and reduces the "atomic resolution" of images obtained in our computer simulation to a "resolution" where these images could be compared with the conventional TEM images. Function (2) assumes the values between 0 and 1. In our pictures, this corresponds to the change in color from the black color, describing the O(I) ordered domains of the first orientation, to the white color, describing the O(I) domains of the second orientation. The gray color corresponds to the disordered state. Using $\langle \eta \rangle$ instead of η results in "smearing" a dopant atom into a small area.

Figure 1(a) demonstrates the temporal evolution of a simulated structure during the "annealing" at the temperature $T_a/T_0=0.79$ at small dopant content $x=0.04$, the reduced time t^* of "annealing" being changed within the range from 4 to 348. At the initial stage of annealing, the $T\rightarrow$O(I) ordering results in appearance of ultrafine domains of two orientation variants of the orthorhombic O(I) phase. These domains form the tweed pattern. Later, the tweed structure transforms into the (110) polytwin structure. Figure 1(b) shows the corresponding strain-induced diffuse scattering around the (400) diffraction spot (the calculated intensity is shown on a logarithmic scale, the details of calculations are given in Ref. 5). Both Figs. 1(a) and 1(b) show the gradual temporal evolution from the tweed structure to the (110) polytwin structure. This is the same type of the evolution as that observed experimentally[36] and predicted theoretically[4,5] for undoped materials. Doping produces the local disorder around the M atoms which is well seen in Fig. 1(a) at large times t^* and in Figs. 2(a) and 2(b). The local disorder in these figures manifests itself as small grey "islands" on the twin boundaries and within the (110) twins.

Figure 2 presents the metastable structures for different x at the same temperature $T_a/T_0=0.79$. The structures are metastable (or, possibly, stable) because they do not practically change after a certain annealing time t_0^*. This time t_0^* strongly depends on the dopant content x. For example, at $x=0.40$, $t_0^*\sim 10$. However, the time t_0^* is about ~ 30, 50, 100, 150, and 300–400 at smaller x values, $x=0.24$, 0.18, 0.12, 0.10, and ≤ 0.08, respectively. We note, that the time t_0^*, necessary to form the final stable twin structure in undoped material ($x=0$), is about 100. This is 3 times less than the time ($t_0^*\sim 300$) that was found necessary to form the twin structure at the small doping, $x=0.04$.

The polytwin structure at $x=0.04$ shown in Fig. 2(a) is the same as in Fig. 1(a) for the time $t^*=348$. Figure 2(a) presents the (110) twins with wide diffuse boundaries and the "point" defects around the positions of dopant atoms. Within the range $\sim 0.1<x<\sim 0.2$, Figs. 2(c)–2(e) show the tweed structure which is similar to that previously observed in the trivalent-doped $YBa_2Cu_{3-x}M_xO_{7-\delta}$ (Refs. 11–14) and to the tweed obtained in this work [Figs. 3(c)–3(e)]. Although the ultrafine orthorhombic domains forming the tweed pattern locally distort the crystal lattice, the average crystal lattice determining the diffraction spot pattern is tetragonal. At further increase of x, the tweed structure gradually transforms into a homogeneous tetragonal phase [Figs. 2(f) and 2(g)].

Results presented in Fig. 2 describe the final microstructures at different x. These microstructures are in a very good agreement with experiment (compare, for example, Fig. 2 with Fig. 3). While the polytwin structure forms at small dopant content, $x<\sim 0.08$, the tweed structure appears at larger x. The approximate border stoichiometry, separating the stability regions of the twin and tweed patterns, is $x_0\sim 0.08$. This stoichiometry is close to the experimental values: $x_0\leq 0.09$ for Fe

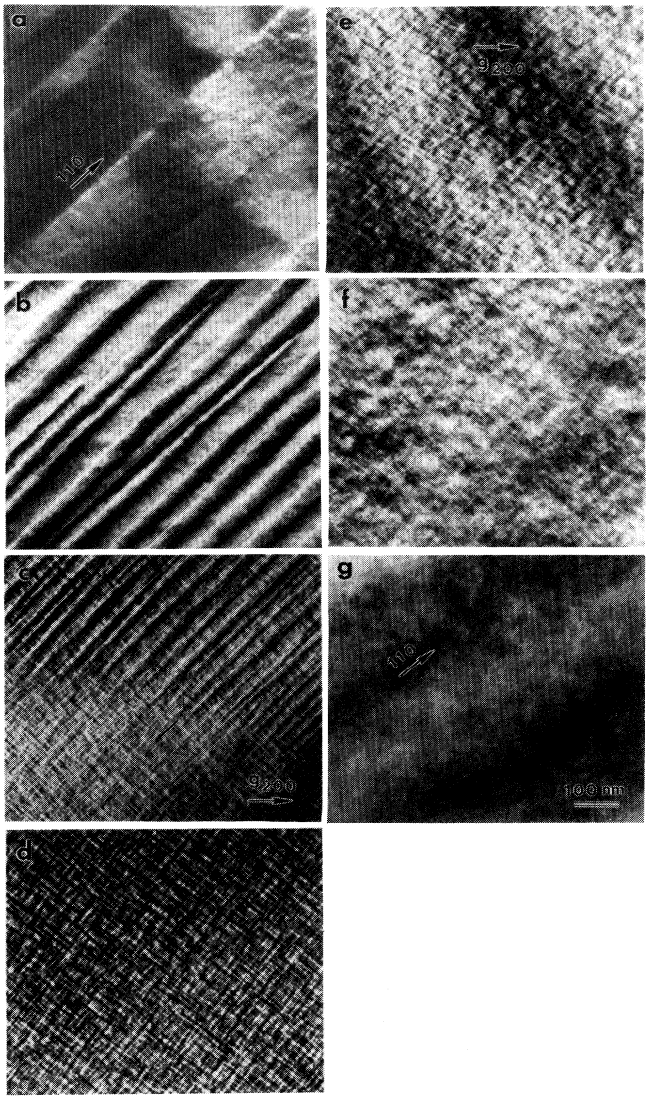

FIG. 3. Morphologies in $YBa_2Cu_{3-x}Fe_xO_{7-\delta}$ obtained by TEM (under $g=200$ two-beam condition) at different dopant content x: (a) 0.045, (b) 0.06, (c) 0.075, (d) 0.09, (e) 0.15, (f) 0.3, and (g) 0.45. All images have the same scale.

doped[11] and $x_0 \sim 0.06-0.07$ for the Co-doped[13,14] $YBa_2Cu_3O_{7-\delta}$. Considering the simplicity of our model (iii) for the M-O interaction, this quantitative agreement is very good. We note, that the value x_0 depends on temperature. It decreases upon lowering the temperature.

III. EXPERIMENTAL RESULTS

The samples of the Fe-dopant oxides, $YBa_2Cu_{3-x}Fe_xO_{7-\delta}$ $(0.045 \leq x \leq 0.45)$, were prepared by mixing the appropriate amounts of Y_2O_3, $BaCO_3$, CuO, and Fe_2O_3 powders in an agate mortar. The ground powders were pressed into pellets and fired in the air at 900 °C twice. They were heated in oxygen at 970 °C for more than 40 h, followed by an anneal at 665 °C for 8 h, and then furnace cooled to below 100 °C. The resulting samples were well crystallized with shiny facets on the interior.

The transmission electron microscopy was performed on a JEM-2000FX electron microscope operated at 200 keV. The majority of the TEM specimens (at least two for each composition) were prepared by slicing the sintered pellets, ultrasonically cutting out the 3 mm disks, mechanically dimpling to ~ 25 μm thick, initially ion milling at 4 keV at 8°–10° tilt, and, finally, milling at a reduced angle of $\sim 6°$ or a reduced voltage of 2 keV. To verify that no artifacts were being introduced during the ion-milling process at room temperature, several specimens of ground pellets suspended on holey carbon films were examined, as well as the samples ion-milled using the liquid-nitrogen-cooled stage. The only observable difference among the specimens prepared by these various methods is that the ion-milling samples had a very thin amorphous layer on the surface.

Figure 3 demonstrates the dependence of the microstructure on the dopant content x. All the images were recorded under $g = 200$ diffraction condition with the same deviation from the Bragg reflection. This figure shows that the tweed pattern appears within the range $\sim 0.075 < x < \sim 0.3$. At small x $(x < \sim 0.075)$, the twins, having the diffuse boundaries and the defect internal structure, are observed. At larger values of x $(x > \sim 0.3)$, we find a more homogeneous structure rather than tweed.

Comparing the electron microscopic images (Fig. 3) and the computer simulated results (Fig. 2) shows that both give the same dependence of microstructure on the dopant atom content x. Both give the same doping range $(\sim 0.08 < x \sim 0.3)$, where the appearance of the tweed microstructure is expected.

We note, that the linear size of the simulated pictures, equal to 128×3.856 Å ~ 50 nm, is about a half of the bar (100 nm) shown on electron microscopic images (Fig. 3). Therefore, the experimental images are approximately 10 times bigger than the computer simulated pictures.

IV. DISCUSSION

As was found in previous experimental studies, doping by atoms with the same valency as Cu(I) atoms (like Ni or Zn) does not affect the atomic structure and mesoscopic morphology of superconducting $YBa_2Cu_{3-x}M_xO_{7-\delta}$. Such influence was found only at doping by trivalent cations (like Fe, Co, or Al). The difference could be interpreted in the light of experimental data.[21,23,25] These works showed that the impurity cation M, whose valency exceeds the valency of a Cu(I) atom, has a greater number of the nearest oxygen atoms. If this is the case, the trivalent dopant atom should produce a local oxygen disorder which certainly should effect the oxygen ordering in $YBa_2Cu_{3-x}M_xO_{7-\delta}$. A reason for this is the following.

Since the character of the Cu-O covalent bonding does not allow a Cu(I) atom to have more than two nearest-neighbor O atoms in the a-b plane, the O atoms in the ordered orthorhombic structure are located on the b-interstitial sites along the b axis, "permitted" in this ordered state. The situation is different for a trivalent M atom. It binds more than two O atoms in the a-b plane. Two of them occupy the two b sites, nearest to the M atom, while the remaining O atoms, binded to the M atom, must occupy the rest of available sites nearest to the M atom. These available sites are the a sites. Since in the ordered state the a sites are not "permitted" for the occupation by oxygen, the appearance of oxygen atoms on these a sites produces the local disorder.

Certain qualitative predictions about the doping effect, which follow from the physical mechanism described above, could be made.

(i) If the concentration of M atoms is sufficiently high, their disordering effect should destabilize the ordered orthorhombic phase and shift the thermodynamic equilibrium towards the disordered tetragonal phase. This is exactly what is observed experimentally at the high dopant stoichiometry x.

(ii) If the concentration of M atoms is low (a small amount of local disordering centers), their effect on an ordering structure is not expected to be substantial and ordering should occur in the same way as in undoped $YBa_2Cu_3O_{7-\delta}$, i.e., by formation of the (110) polytwin structure via the transient tweed structure. However, even in this case, the local disordering may play a role of pinning centers for boundaries between the domains of two orientation variants of the ordered orthorhombic phase. Pinning the domain boundaries may adversely affect coarsening of the polytwin structure and, thus, may be responsible for observation of considerably thinner (110) twins upon further doping within this stoichiometry range.

(iii) In intermediate range of the M-atom concentration, the pinning effect of the local disorder may be so considerable that the tweed→twin transition, requiring the domain boundary mobility, becomes impossible. If this is the case, the stable tweed structure should be observed.

These qualitative conclusions following from the nearest-neighbor M-O attraction [model (iii)] for trivalent dopant M atoms agree well with the new TEM observations (Fig. 3) and the previous electron microscopic data.[11–14] They also agree with our computer simulation, for the M-O nearest-neighbor attraction, which provides a numerical characterization of the multiparticle nonlinear diffusion process of interacting oxygen atoms.

The simulation demonstrates that dopant atoms produce the local disorder areas around them [these areas appear as the small grey areas in Fig. 1(a), at large time t^*, and in Figs. 2(a) and 2(b)]. It also shows that the additional M-O attractive interaction is mostly responsible for the specific structure characteristics of $YBa_2Cu_3O_{7-\delta}$ doped by trivalent cations. It is interesting that even this simplified two-dimensional model assuming the pairwise M-O nearest-neighbor attractive interaction together with the long-range O-O interactions, anisotropic electrostatic[32,33] and strain-induced,[1,3] produces the structures which are in a very good agreement with the electron microscopic observations. The latter could be, particularly, illustrated by comparison of the simulated structures (Fig. 2) with the TEM images (Fig. 3). The simulated structures show an excellent resemblance to the observed structures on the TEM images. And what is more, they correctly reproduce the transition from the twin structure at small M content to the tweed structure at higher M content and the transition from the tweed structure to a disordered tetragonal phase at very high M content.

Surprisingly, this simple model gives even good quantitative predictions. It predicts the correct value for the "critical" stoichiometry x_0 which separates the twin and tweed stoichiometry fields. Indeed, as was mentioned above, the value of x_0 following from the computer simulation is about 0.08, whereas the experimental values of x_0 for Fe- and Co-doped $YBa_2Cu_3O_{7-\delta}$ vary within the range 0.06–0.09.[11,13,14] The simulation shows that the tweed structure disappears at the stoichiometries above the second "critical" stoichiometry $x_1 \sim 0.3$. At $x > x_1 \sim 0.3$, a homogeneous tetragonal (disordered) phase is formed [see Fig. 2(g)]. The experimental observations give approximately the same critical stoichiometry $x_1 \sim 0.3$. The obtained agreement seems to indicate that our model of the O-O and M-O interactions, regardless of all its obvious oversimplifications, correctly grasps the main physics of the phenomenon.

It is natural to raise a question, whether the computer simulation results are sensitive to variation of the M-O potential. In this work, we have investigated the effect of the long- and short-range M-O interactions on the structure formation [models (i)–(iii)]. As was mentioned above, the simulations with the long-range M-O interactions (electrostatic and strain induced) are not able to produce the observed metastable tweed structures at all. This result can be readily interpreted in the light of the fact that the long-range M-O interaction would not generate the local disorder discussed above. Indeed, if the M-O attraction is long-range, the argument about the local disorder, presented in the beginning of this section, is not applicable because there is no need for the extra O atoms to be attracted (by an M atom) to its nearest-neighbor a sites. Extra O atoms, attracted into a large M-O interaction radius sphere, have a choice to occupy the "permitted" b sites beyond the nearest coordination shell around the M atom. In this case, no local disorder is introduced. The M-O strain-induced interaction, being long-range, also does not give a local disorder. Therefore, we can conclude that only the nearest-neighbor M-O interaction is responsible for appearance of the metastable (or stable) tweed structure in $YBa_2Cu_{3-x}M_xO_{7-\delta}$. This analysis agrees with the fact that the trivalent dopant atoms have a substantial covalent contribution to bonding with oxygen atoms which is always short-range.

Several comments concerning the O-O interaction in this system could also be made. Although the M-O nearest-neighbor attraction, in principle, can provide the stable (or metastable) mesoscopic structure formed by ordered domains, it, however, cannot generate the typical $\langle 110 \rangle$ alignment which is a fingerprint of the tweed pattern. The alignment can be obtained only if the long-range strain-induced O-O interaction is taken into account. Therefore, the observation of the tweed structure in $YBa_2Cu_{3-x}M_xO_{7-\delta}$ conclusively demonstrates that the strain-induced interaction between oxygen atoms plays a fundamental role in this system and, thus, cannot be ignored.

As for the long-range electrostatic interaction between the oxygen atoms assumed in our model, the tweed structure could be, in principle, obtained without it. However, any short-range interaction model for the O-O potential would be unsatisfactory because it fails to explain the appearance of the observed long-period structures reported in undoped $YBa_2Cu_3O_{7-\delta}$ (the short-range interaction cannot provide their stability).

In spite of the good agreement between the simulated and observed structures, there is a technical shortcoming related to a limited size of the computational cell. Particularly, we cannot obtain the effect of rapid decrease of the twin spacing upon doping at small x, which is observed experimentally in Refs. 11–14 and in our Figs. 3(a) and 3(b). The reason for this is the following. The thickness of the "thick" twins obtained in our computer simulations cannot be bigger than the size of our computational cell (128×128). But this size is of the same order of magnitude as the thickness of the thinnest lamellar twins observed experimentally. Therefore, to describe the more thick twins, the computer simulation should be performed on a computational cell which is substantially bigger than the cell (128×128) used in this work. However, it can hardly be done at the current status of the supercomputing.

V. CONCLUSIONS

(1) The proposed simple theoretical model provides a good agreement between the calculated and observed structures in the $YBa_2Cu_{3-x}M_xO_{7-\delta}$ doped by trivalent cations M.

(2) To describe the mesoscopic tweed structure, the long-range strain-induced O-O interaction and the nearest-neighbor dopant-oxygen attraction should be introduced. The long-range dopant-oxygen interaction does not produce the tweed structure.

(3) The nearest-neighbor dopant-oxygen attraction results in a local disorder. The local disorder, introduced by dopant atoms, and the strain-induced O-O interaction are the key factors in the formation of the stable/metastable mesoscopic tweed structure and in its transformation to the disordered tetragonal structure at

high dopant content. This conclusion is, probably, correct for many other ordering systems as well.

ACKNOWLEDGMENTS

We gratefully acknowledge the support by Division of Materials Science, U.S. Department of Energy, under Grant No. DE-FG05-90ER45430 and the support by Offices of Basic Energy Sciences under Contract No. DE-AC02-76CH00016. The simulation was performed on CONVEX, SRAC, College of Engineering, Rutgers University, and on Cray-YMP at the Pittsburgh Supercomputing Center.

[1]A. G. Khachaturyan and G. A. Shatalov, Zh. Eksp. Teor. Fiz. **56**, 1037 (1969) [Sov. Phys. JETP **29**, 557 (1969); Acta Metall. **23**, 1089 (1975).

[2]A. L. Roitburd, Fiz. Tverd. Tela (Leningrad) **10**, 619 (1969) [Sov. Phys. Solid State **10**, 2870 (1969)].

[3]A. G. Khachaturyan, *The Theory of Structural Transformation in Solids* (Wiley, New York, 1983).

[4]S. Semenovskaya and A. G. Khachaturyan, Phys. Rev. Lett. **67**, 2223 (1991).

[5]S. Semenovskaya and A. G. Khachaturyan, Phys. Rev. B **46**, 6511 (1992).

[6]L. E. Tanner, Philos. Mag. **14**, 111 (1966).

[7]D. E. Laughlin, R. Sinclair, and L. Tanner, Scr. Metall. **14**, 373 (1980).

[8]I. M. Robertson and C. M. Wayman, Philos. Mag. A **48**, 421 (1983); **48**, 443 (1983); **48**, 629 (1983).

[9]S. Wen, A. Khachaturyan, and J. W. Morris, in *Modulated Structures–1979 (Kailua Kona, Hawaii)*, Proceedings of the International Conference on Modulated Structures, AIP Conf. Proc. No. 53, edited by J. M. Cawley, J. B. Cohen, M. B. Salamon, and B. J. Wuensch (AIP, New York, 1979).

[10]S. Wen, A. Khachaturyan, and J. W. Morris, Metall. Trans. **12A**, 581 (1981).

[11]Youwen Xu, M. Suenaga, J. Tafto, R. L. Sabatini, A. R. Moodenbaugh, and P. Zolliker, Phys. Rev. B **39**, 6667 (1989).

[12]Yimei Zhu, M. Suenaga, and A. R. Moodenbaugh, Ultramicroscopy **37**, 341 (1991).

[13]W. W. Schmahl, A. Putnis, E. Salje, P. Freeman, A. Graeme-Barber, R. Jones, K. K. Singh, J. Blunt, P. P. Edwards, J. Loram, and K. Mirza, Philos. Mag. Lett. **60**, 241 (1989).

[14]R. Wordenweber, G. V. S. Sastry, K. Heinemann, and H. C. Freyhardt, J. Appl. Phys. **65**, 1648 (1989).

[15]T. Siegrist, L. F. Schneemeyer, J. V. Waszczak, N. P. Singh, R. L. Opila, B. Batlogg, L. W. Rupp, and D. W. Murphy, Phys. Rev. B **36**, 8365 (1987).

[16]J. M. Tarascon, P. Barboux, P. F. Miceli, L. H. Greene, G. W. Hull, M. Eibschutz, and S. A. Sunshine, Phys. Rev. B **37**, 7458 (1988).

[17]P. F. Miceli, J. M. Tarascon, L. H. Greene, P. Barboux, F. J. Rotella, and J. D. Jorgensen, Phys. Rev. B **37**, 5932 (1988).

[18]J. F. Bringley, T.-M. Chen, B. A. Averill, K. M. Wong, and S. J. Poon, Phys. Rev. B **38**, 2432 (1988).

[19]P. Bordet, J. L. Hodeau, P. Strobel, M. Marezio, and A. Santoro, Solid State Commun. **66**, 435 (1988).

[20]P. Zolliker, D. E. Cox, J. M. Tranquada, and G. Shirane, Phys. Rev. B **38**, 6575 (1988).

[21]C. Y. Yang, S. M. Heald, J. M. Tranquada, Youwen Xu, Y. L. Wang, A. R. Moodenbaugh, D. O. Welch, and M. Suenaga, Phys. Rev. B **39**, 6681 (1989).

[22]R. S. Howland, T. H. Geballe, S. S. Laderman, A. Fischer-Colbrie, M. Scott, J. M. Tarascon, and P. Barboux, Phys. Rev. B **39**, 9017 (1989).

[23]F. Bridges, J. B. Boyce, T. Claeson, T. H. Geballe, and J. M. Tarascon, Phys. Rev. B **39**, 11 603 (1989).

[24]S. Katsuyama, Y. Ueda, and K. Kosuge, Physica C **165**, 404 (1990).

[25]C. Y. Yang, A. R. Moodenbaugh, Y. L. Wang, Youwen Xu, S. M. Heald, D. O. Welch, M. Suenaga, D. A. Fischer, and J. E. Penner-Hahn, Phys. Rev. B **42**, 2231 (1990).

[26]J. V. Andersen, N. H. Andersen, Ole G. Mouritsen, and H. F. Poulsen (unpublished).

[27]Zhi-Xiong Cai, Yimei Zhu, and D. O. Welch, Phys. Rev. B **46**, 11 014 (1992).

[28]G. Baumgartel and K. H. Bennemann (unpublished).

[29]Yimei Zhu, M. Suenaga, and A. R. Moodenbaugh, Philos. Mag. Lett. **62**, 51 (1990).

[30]Y. Zhu, M. Suenaga, and J. Tafto, Philos. Mag. Lett. **64**, 29 (1991).

[31]Y. Zhu, M. Suenaga, and J. Tafto, Philos. Mag. A (to be published).

[32]A. A. Aligia, A. G. Rojo, and B. R. Alascio, Phys. Rev. B **38**, 6604 (1988).

[33]A. A. Aligia, J. Garces, and H. Bonadeo, Phys. Rev. B **42**, 10 226 (1990).

[34]R. J. Cava, B. Batlogg, C. H. Chen, E. A. Rietman, S. M. Zahurak, and D. Werder, Nature **329**, 423 (1987).

[35]R. C. Baetzold, Phys. Rev. B **38**, 11 304 (1988).

[36]G. Van Tendeloo and S. Amelinckx, J. Electron Microsc. Tech. **8**, 285 (1988).

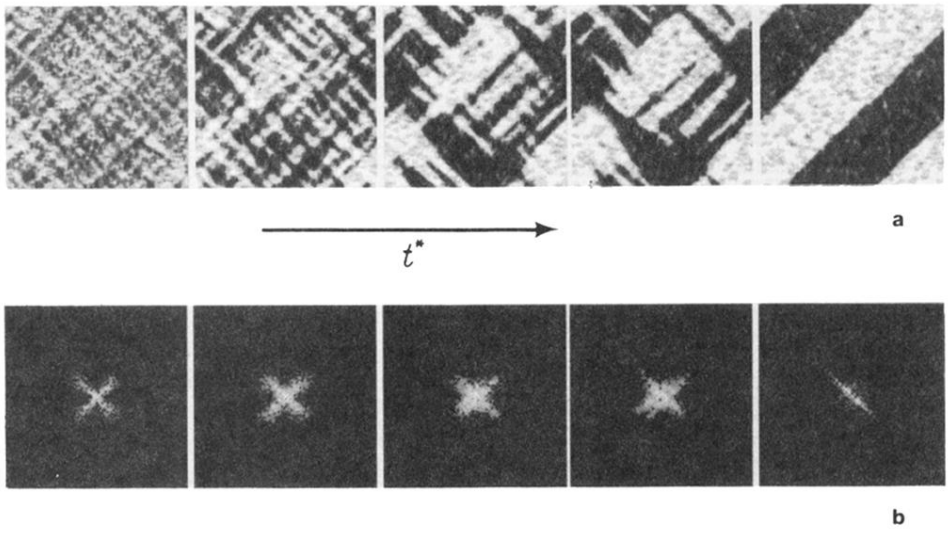

FIG. 1. (a) Simulated temporal isothermal evolution of microstructure in doped $YBa_2Cu_{3-x}M_xO_7$ at $x=0.04$ and the temperature $T_a/T_0=0.79$. The transformation reduced time t^* is equal: 4, 8, 48, 108, 348 (from left to right). The transient tweed structure (at small times $t^*=4$ and 8) obtained along the transformation path from the initial disordered state transforms to the (110) twinned ordered state, therefore, showing the tweed→twin rearrangement. Two types of orientation domains are characterized by the value of the lro parameter $\langle \eta \rangle$ [Eq. (2)]. Black and white colors describe the O(I) ordered domains of two different orientations. Small gray areas are around the positions of dopant atoms. (b) The corresponding strain-induced diffuse scattering around (400) fundamental diffraction spot. The intensity is shown on a logarithmic scale. The system size is 128×128 unit cells.

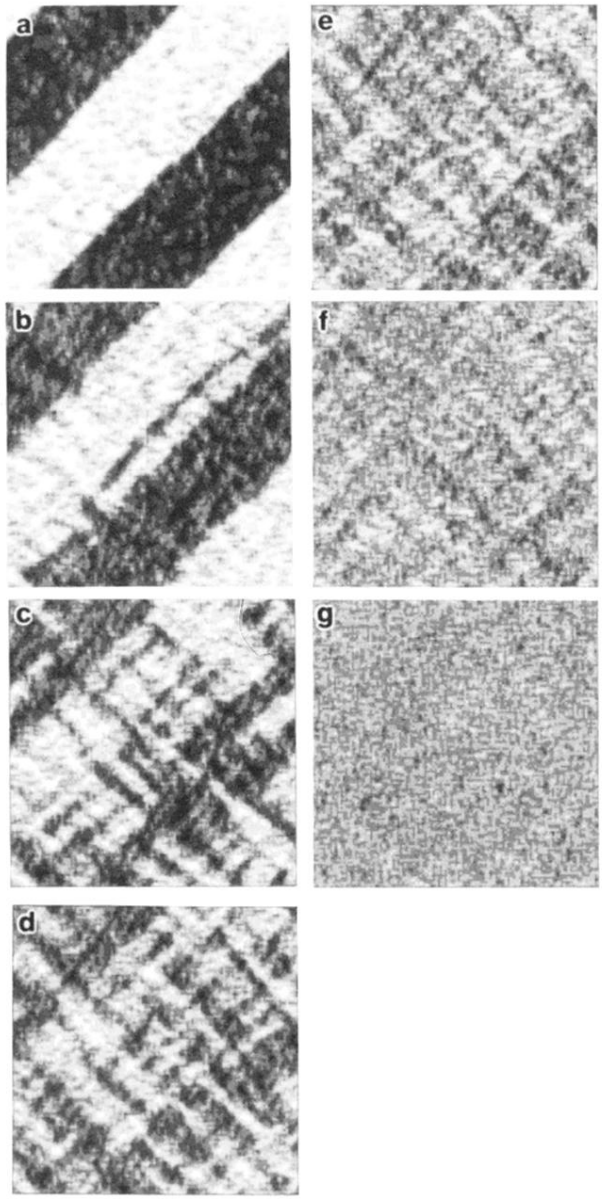

FIG. 2. Simulated microstructures in $YBa_2Cu_{3-x}M_xO_7$ at different dopant content x at the temperature $T_a/T_0=0.79$. The values of x are (a) 0.04, (b) 0.08, (c) 0.10, (d) 0.12, (e) 0.18, (f) 0.24, and (g) 0.40. The transformation reduced time t^* is equal to (a) 348, (b) 408, (c) and (d) 188, (e) 168, and (f) and (g) 48. All conditions are the same as for Fig. 1(a).

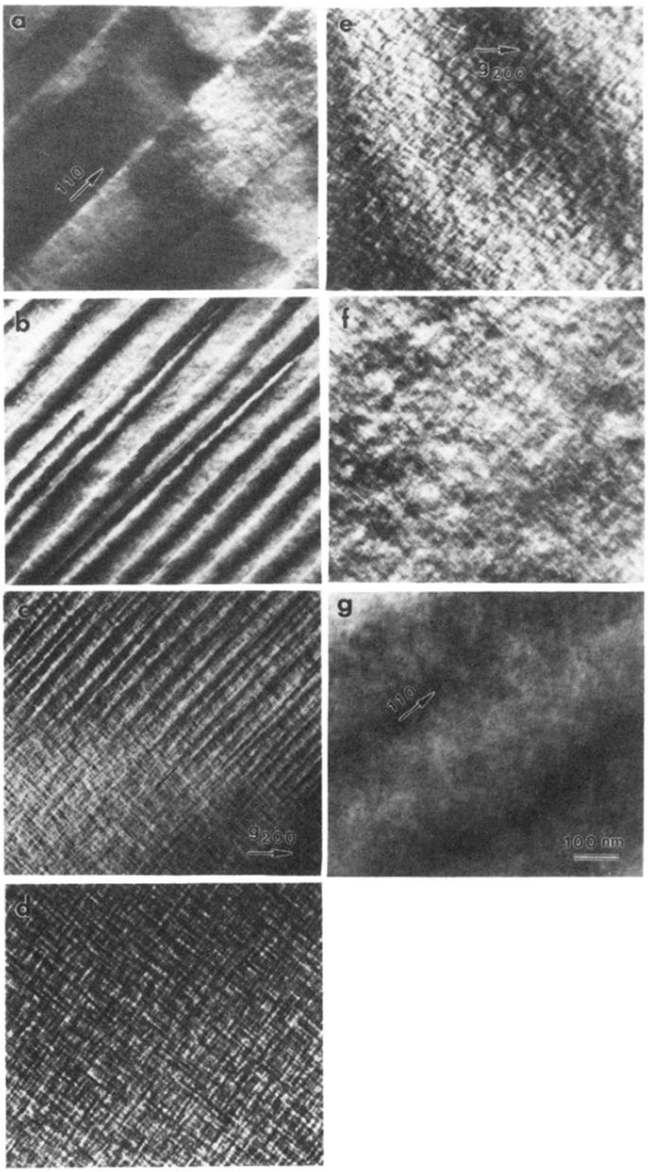

FIG. 3. Morphologies in $YBa_2Cu_{3-x}Fe_xO_{7-\delta}$ obtained by TEM (under $g=200$ two-beam condition) at different dopant content x: (a) 0.045, (b) 0.06, (c) 0.075, (d) 0.09, (e) 0.15, (f) 0.3, and (g) 0.45. All images have the same scale.